

Fully Automatic Renal Parenchyma Volumetry in LDA-based Probability Maps Using Variational Outer Cortex Edge Alignment Forces

Oliver Gloger¹, Klaus Tönnies², Volkmar Liebscher³, Henry Völzke¹

¹Ernst Moritz Arndt University of Greifswald, Institute for Community Medicine, Walther-Rathenau-Str. 48, 17475 Greifswald, Germany

²Otto-von-Guericke University of Magdeburg, Institute for Simulation and Graphics, Universitätsplatz 2, 39106 Magdeburg, Germany

³Ernst Moritz Arndt University of Greifswald, Institute for Mathematics, Walther-Rathenau-Str. 47, 17475 Greifswald, Germany

Abstract. The development of fully automatic 3D segmentation techniques for abdominal organs in magnetic resonance (MR) datasets is a very challenging task in the domain of medical image analysis. Especially, for surgical applications and epidemiological studies well-designed segmentation strategies are required that incorporate intensity information of all available MR contrasts as well as edge information of organ frontiers. Prior organ shape information can be used to assist delineation between adjacent organs. In this work a variational edge alignment force is proposed to guide prior shape level set segmentation to outer organ frontiers. The edge alignment force is developed and tested for an existing 3D level set approach to segment renal parenchyma in MR datasets for an epidemiological study. Furthermore, the existing approach is extended to use additional parenchyma features of all MR contrasts for segmentation. MR-intensity information of all MR contrasts are incorporated in probability maps, which are generated by using discriminant reduction techniques combined in a probabilistic Bayesian approach. A method to calculate probability maps in proband-specific kidney regions is presented. The presented extensions improve volumetric renal parenchyma results but can also be applied to segment other organs in MR datasets.

Keywords: variational image segmentation, level sets, linear dimension reduction, Bayesian theorem

1 Introduction

Advanced imaging techniques offer many possibilities to assist (bio)medical applications like surgical planning and modern diagnosis. However, medical imaging techniques produce large amounts of medical data, which often requires elaborate tissue and organ segmentation by medical experts. In community medicine, medical image segmentation enables quantification of certain health-related properties in populations accelerating research insights in the domain of modern epidemiological science. This work is designed for renal parenchyma volumetry in an epidemiological study, in which MR data of probands are used to develop scientific findings about population-based health properties concerning renal tissue functions. The algorithms, however, can also be applied in the clinical setting, where large numbers of patients undergo MR examinations. Since manual organ segmentation is very time-consuming and cannot be accomplished by radiologists in hospitals, automatic methods have to support organ segmentation in MR data. A new technique for probability map generation in proband-adapted segmentation regions for renal parenchyma tissue is proposed in this approach. Furthermore, a supporting variational outer cortex edge alignment force for more exact parenchyma volumetry in MR data is proposed. The used prior shape segmentation combined with the proposed variational outer organ edge force can also be applied to segment other organs.

2 Related Work

The literature shows that there exist several kidney segmentation approaches for CT data [1]-[4], but only very few for MR data, and previous work for MR data is developed for contrast enhanced MR examinations. For these type of MR data, graph cut techniques are used in [5] and in [6]. Contrast-enhanced MR time series are applied in [7] to segment rat kidneys. Song et al. [8] use a combined registration and segmentation method to segment 4D time series of contrast-enhanced MR images. The authors in [9] propose a deformable model, which combines signed distance map densities with grey value distributions calculated by an expectation maximization algorithm. However, those techniques for contrast enhanced MR data as well as existing work for CT data are not suitable for native MR data sets of large-scale epidemiological studies, where contrast enhanced MR methods are rarely applied for ethical reasons. Furthermore, existing approaches for MR data are designed for kidney segmentation but not for automatic volumetry of renal parenchyma, which requires to recognize and to exclude renal pelvis. The work of [10] proposes a fully automatic renal parenchyma segmentation framework. Prior shape level set segmentation is applied in stepwise refined 3D renal parenchyma probability maps and extended by stopping and attraction forces to fix the zero level set at outer parenchyma edges. This work applies several methods of [10] and proposes three extensions to improve the results for renal parenchyma volumetry. Since in [10] the authors use only a single MR contrast to generate probability maps, we propose an extended approach incorporating all available MR contrasts for probability map generation. This extension in-

creates the number of parenchyma features for more successful segmentation. We develop a method to calculate proband-adapted regions, in which renal parenchyma tissue of individual probands is most likely located. Furthermore, we derive an outer cortex edge alignment force by using variational techniques, which results in a single attraction term.

3 MR Data Acquisition

Four different datasets were created using the VIBE (volume interpolated breath-hold exam) sequence (Fig.1). The T1-weighted VIBE sequence [11] provides in- and out-phase as well as water- and fat-saturated images. $TR = 7.5$ (ms) and multimodal $TE = 2.4/4.8$ (ms) have been used in context with a flip angle of 10° . The voxel size is $1.64 \times 1.64 \times 4.0$ mm and the scan time has been 19 (s) for 64 slices.

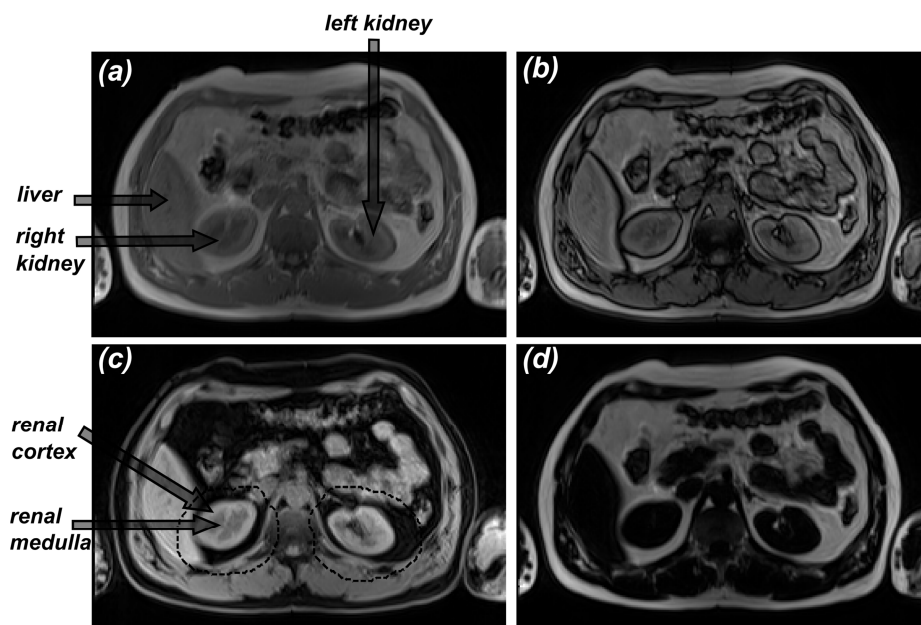


Fig. 1. Original MR images taken from a transversal slice of the VIBE measurements with selected organs and tissue types relevant for MR parenchyma segmentation marked in the images. (a) Normal weighting, (b) opposed-phase weighting, (c) fat-saturated weighting with MLKR for both kidneys depicted by dashed black contours, (d) water-saturated weighting. Frequently mentioned organs and tissue types in this work are labelled.

4 Description of the Method

4.1 Training Phase Description

Medical experts selected 50 denoised MR data sets of different probands and performed manual segmentations for training which resulted in saved binary parenchyma masks. Regions for left and right parenchyma are determined as set unions of trained parenchyma masks, which contain most probably all parenchyma tissue of the probands of the study and are the most likely kidney regions (MLKR). Background voxels inside the MLKR (s. Fig.1 (c)) and in the vicinity of the renal parenchyma, that not belong to the parenchyma tissue, are stored in a parenchyma-background mask. Furthermore, liver masks and renal cortex masks for left and right kidneys are generated and saved. Samples are generated from the stored binary masks. Different to [10] the collected samples in this work consist of vector voxels representing the four different MR-weightings. Furthermore, characteristic 2D horseshoe-like forms of left and right parenchyma that can be found in inner transversal parenchyma slices are selected from the 50 training MR datasets and segmented manually by medical experts. Recognition of parenchyma forms using their inner horseshoe-like 2D forms supports the proposed refinement techniques of [10]. The parenchyma shape is represented as a trained signed distance map of the segmented regions and used in the prior shape level set segmentation step in combination with the method of [12].

4.2 MLKR Refinement

The MLKRs of both kidneys are refined to exclude regions inside the MLKRs that most probably are no renal parenchyma regions. All trained renal parenchyma masks are aligned according to their centroids and the union set of all aligned parenchyma masks are stored in the database. We apply the Fourier descriptor method of [10] to recognize 2D horseshoe forms which are characteristic forms of inner transversal renal parenchyma slices. Hence, we use the centroid of all recognized horseshoe forms of a new proband as estimation of the proband's renal parenchyma centroid. The stored union set of the aligned training shapes in the database is then aligned with the estimated centroid of the proband (Fig.2). The refined MLKRs (ref_MLKRs) are proband-adapted kidney regions to reduce possible oversegmentations into non-parenchyma regions in subsequent segmentation steps. The ref_MLKRs are better adapted to the individual parenchyma regions of the probands' MR datasets than the MLKRs proposed in [10].

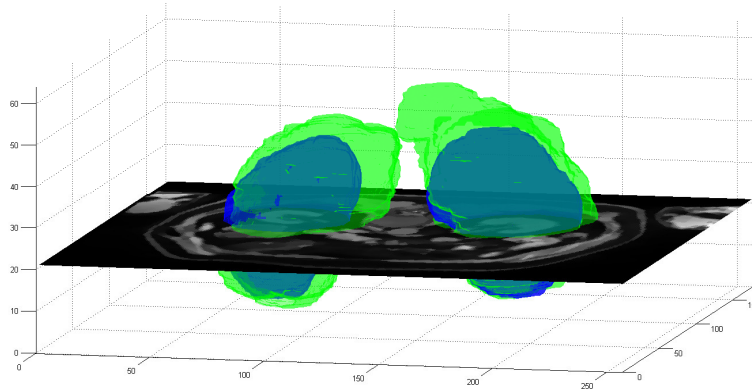


Fig. 2. MLKRs for left and right kidney as overlap regions of 50 trained parenchyma masks (green) and ref_MLKR (blue).

4.3 Probability Map Generation

Two different probability maps are calculated and used for further segmentation steps. The collected samples of the renal parenchyma and the parenchyma-background samples inside the MLKR are used to generate parenchyma probability maps. Additionally, liver-cortex probability maps for the whole MR data set region are calculated from the samples of the liver-cortex masks and their background masks. They are used for further parenchyma probability map refinement and for assisting the final level set segmentation step using the proposed, variationally derived segmentation force. Opposed to [10], who use only a single MR-weighting, we incorporate all the four available MR-weightings and combine dimension reduction with probability map generation. Linear discriminant analysis (LDA) [13] is used for linear dimension reduction (LDR), which reduces the dimensionality (n) of the samples from $n=4$ to $n=1$ by preserving as much discriminant information between the given class distributions as possible in linear manner.

Dimension reductions are performed for the two-class case of parenchyma and its background as well as for the two-class case of liver-cortex and its background. Histograms of the projected data are determined, which are smoothed using a convolution with a Gaussian kernel with standard deviation of 3.0. For both probability map generations the smoothed histograms are used to determine the likelihoods for the Bayesian theorem. Consequently, parenchyma probability maps inside the MLKR are determined by:

$$P_{rpc} = P(rpc | I_{LDR}) = \frac{p(I_{LDR} | rpc) \cdot pr(rpc)}{p(I_{LDR} | rpc) \cdot pr(rpc) + p(I_{LDR} | bg_rpc) \cdot pr(bg_rpc)} \quad (1)$$

where $ILDR = ILDR(x,y,z)$ is the projected value onto the projection axis of the LDA calculated between parenchyma and parenchyma-background tissue for the vector voxel at position (x,y,z) in the MR dataset. $p(ILDR|rpc)$ and $p(ILDR|bg_rpc)$ are the like-lihoods determined by the smoothed histograms of the projected data. The a priori probabilities $pr(rpc)$ of parenchyma and $pr(bg_rpc)$ of the parenchyma-background are determined by calculating their ratios in the MLKR of the trained binary masks. Similarly, liver-cortex probability maps are generated using a priori probabilities $pr(lctx)$ for liver-cortex and $pr(bg_lctx)$ for the background, determined by ratios of their sample occurrences inside the whole MR dataset region:

$$P_{lctx} = P(lctx | I_{LDR}) = \frac{p(I_{LDR} | lctx) \cdot pr(lctx)}{p(I_{LDR} | lctx) \cdot pr(lctx) + p(I_{LDR} | bg_lctx) \cdot pr(bg_lctx)} \quad (2)$$

In this formula $ILDR$ are the projected values after projection onto the projection axis that is calculated for the samples of the liver-cortex and the background classes. Compared to the probability map generation presented in [10], the $Prpc$ map quality for usage in following segmentation steps is slightly improved (Fig. 3 (a) and (c)). However, the $Plctx$ map quality is improved significantly showing clearer enhanced cortex tissue, which is a particular prerequisite to use outer cortex edge alignment forces in level set segmentation (Fig. 3 (b) and (d)). Furthermore, the probability map results show, that relevant information of parenchymal tissue types is well preserved by applying the proposed reduction technique.

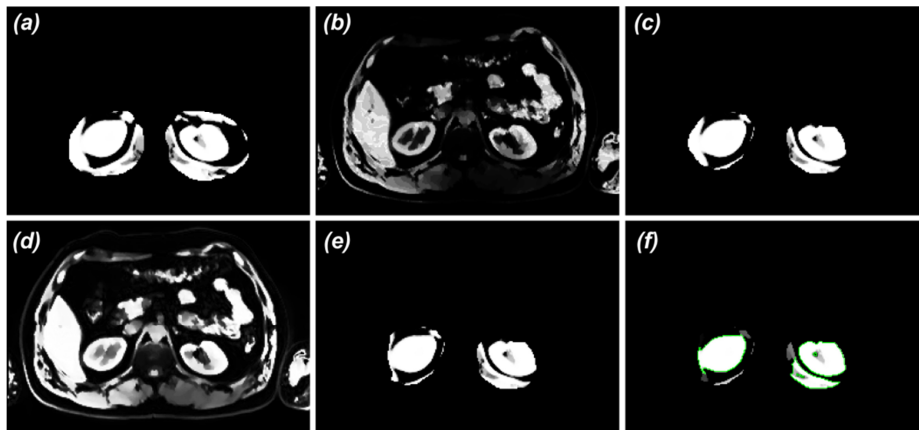


Fig. 3. Parenchyma probability map inside MLKRs (a) and liver-cortex probability map (b) produced by the method of [10]. Parenchyma probability map inside ref_MLKRs (c) and liver-cortex probability map (d) produced by using (1) and (2) respectively. (e) Parenchyma probability map of (c) reduced by recognized liver part, (f) refined parenchyma probability map with modified probability values. The boundary of the starting surface for level set segmentation in the selected slice is also depicted. All results are presented according to the selected proband and slice of figure 1.

Liver part removal requires liver-cortex probability map generation for the whole MR data set region, since maximal cortex extensions are determined to distinguish liver from cortex tissue on distance maps of binary liver-cortex datasets. The liver in the binary liver-cortex datasets is then approximated to remove it in the parenchyma probability maps (Fig.3 (e)). Furthermore, probability map refinement in [10] uses a shrinkage algorithm in signed distance maps of binary parenchyma datasets to cause label separations. Labels depicting parenchyma voxels are recognized by using Fourier descriptors of label boundaries in transversal slices that show the most similarities to the Fourier descriptors of the trained 2D horseshoe forms. Parenchyma probability maps are refined by reducing the probability values of separated labels according to the shrinkage distance, when their separation from the parenchyma including label occurred. This refinement technique incorporates knowledge about the degree of tissue connections between parenchyma regions and low connected non-parenchyma regions (Fig. 3(f)). The surface of the remaining parenchyma including label, which is not separated by this algorithm, serves as suitable starting surface for the following level set segmentation step.

4.4 Prior Shape Level Set Segmentation Using Variational Outer Cortex Edge Alignment

The result of the previous step may still be erroneous (s. Fig. 3 (f)). Thus, a final segmentation step is necessary to improve segmentation results. A level set segmentation method using prior shape knowledge [12] is adapted as final step for parenchyma segmentation. In [12] an energy functional consisting of a data-driven term (originally proposed in [14]) and a shape-driven term is proposed to perform segmentation. For this work, refined parenchyma probability maps are used as data-driven term and signed distance functions based on the surface of the binary training masks are used as prior knowledge of parenchyma shapes. The method proposed in [14] is based on intrinsic alignment, which means, that trained signed distance functions and evolving level set functions are compared by overlaying them according to their centroids. However, shape-driven and data-driven forces can have counteracting values producing oscillations, which will often result in local minima. Furthermore, in [10] it has been shown, that prior shape level set segmentation based only on intrinsic alignment may result in local minima that can be improved by using edge information of renal cortex tissue. Since in [12] and [14] variational formulations are used, in this work a variational formulation is derived for an improved outer cortex edge alignment. This results in a single force that can easily be combined with the approach of [12]. For the intended minimization the following energy functional containing the level set function is used:

$$E(\phi, \nabla\phi) = \iint_{\Omega} -\delta_{chs}(\phi) \cdot \max\left(\left(\nabla\phi + \nabla P\right)^2 - T, 0\right) d\Omega \quad (3)$$

To remove counteracting forces in negative distance regions near the zero level set, we use a modified version of the regularized Dirac function $\delta_\varepsilon(\phi)$ (originally proposed in [14]), which continues constantly into regions with negative distance values:

$$\delta_{\varepsilon hs}(\phi) = \begin{cases} \frac{\varepsilon}{\pi \cdot (\varepsilon^2 + \phi^2)} & , \phi \geq 0 \\ 1 / (\pi \cdot \varepsilon) & , otherwise \end{cases} \quad (4)$$

The gradients of the cortex probability maps are normalized by $\nabla P = \nabla P_{\text{cortex}} / |\nabla P_{\text{cortex}}|$ and reinitialization of the level set function produces normalized gradients $\nabla \phi$. This functional optimizes in regions of positive distance values adjacent to the zero level set the alignment between normalized cortex probability map gradients ∇P and gradients of the signed distance function $\nabla \phi$. The co-domain of the quadratic term lies in the range $[0;4]$ and is influenced by the dot product of the normalized gradients. The more the gradients point in the same direction, the higher is the value of the quadratic term. Experiments show that the optimization using only the quadratic term $(\nabla \phi + \nabla P)^2$ instead of the maximum function in (3) may also result in local minima, where gradients have opposed directions. Thus, the effect of opposed directed gradients is removed by using a maximum function and the threshold $T=2$, which optimizes alignments of gradients directed into same directions. Since previous segmentation steps result very often in starting surfaces that encircle parenchyma tissue, the threshold of $T=2$ can be used to extract probability map gradients, that are aligned in the same direction with the signed distance map gradients and represent most probable outer cortex edges. The minimization of this functional is used to fix the zero level set in a small neighbourhood of the outer cortex edges. For minimization, the *Euler-Lagrange* equation can be calculated (using $M = (\nabla \phi + \nabla P)^2 \geq T$):

$$\delta_\varepsilon(\phi) \cdot (\phi \geq 0) \cdot \frac{-2\phi}{\varepsilon^2 + \phi^2} \cdot \max((\nabla \phi + \nabla P)^2 - T, 0) - 2M \cdot \sum_{i=1}^3 \left[\delta_\varepsilon(\phi) \cdot (\phi \geq 0) \cdot \frac{-2\phi_{x_i}}{\varepsilon^2 + \phi^2} \cdot (\phi_{x_i} + P_{x_i}) + \delta_{\varepsilon hs}(\phi) \cdot (\phi_{x_i x_i} + P_{x_i x_i}) \right] = 0 \quad (5)$$

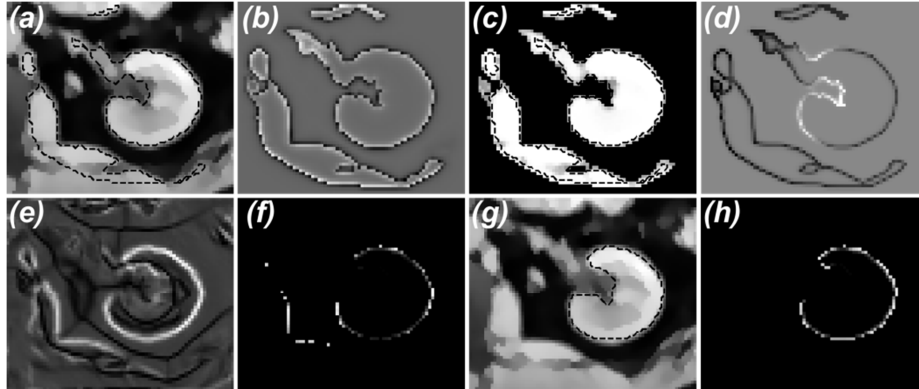


Fig. 4. Example of involved 3D forces shown for a 2D slice: (a) Fatsaturated MR-slice with zero level set depicted as dashed contour at the beginning of the level set segmentation. Data-driven force (b) controlled by the refined probability map of (c) and shape-driven force (d) at the beginning of level set segmentation. (e) Enhanced outer cortex edges produced by the quadratic term $(\nabla\phi + \nabla P)^2$ of the proposed energy functional and (f) resulting outer cortex edge alignment force according to (5) at the beginning of level set segmentation. Final segmentation result in MR-slice (g) and final alignment force (h).

By using gradient descent, (5) represents the outer cortex edge alignment force and can easily be combined with the shape-driven and data-driven forces of [12] and [14]. These three contributing forces in the final level set segmentation step are illustrated in Fig. 4. All forces are normalized and can be weighted individually. We tested several weighting parameters empirically and found an appropriate value of 1.0 for all weighting parameters.

5 Results

We use to different quality measures to evaluate our results. In addition to the Dice coefficient (6), the volume error (7) is listed in Table 1, since the calculated parenchymal volume is used for further epidemiological investigations:

$$DICE = \frac{2 \cdot N(M_T \cap M_S)}{N(M_T) + N(M_S)} \quad (6)$$

$$VE = |V_s - V_T| / V_S \quad (7)$$

The dice coefficient and volume error is determined by comparing the voxel numbers (N) of automatically segmented binary masks (M_S) with manually segmented binary masks (M_T) of medical experts. Similarly, the volume error is calculated using trained volumes (V_T) of medical experts and automatically segmented volumes (V_S).

Table 1. Listed mean and standard deviations (Std) for volume error (VE) and DICE-coefficient as quality measures for segmentation results for left and right parenchyma. Results of the work of [10] are listed in the upper table part for comparison. Segmentation results for the proposed work are shown in the lower table part.

	<i>Renal Parenchyma Segmentation Method of [10]</i>			
	Right Parenchyma		Left Parenchyma	
	VE	DICE	VE	DICE
Mean:	0,075	0,903	0,107	0,893
Std:	0,053	0,033	0,070	0,039
	<i>Our Method</i>			
	Right Parenchyma		Left Parenchyma	
	VE	DICE	VE	DICE
Mean:	0,064	0,920	0,088	0,911
Std:	0,048	0,031	0,083	0,047

The results show that the three proposed extensions improve the fully automatic volumetry results for right and left renal parenchyma. In general, segmentation results for left parenchyma are worse than for right parenchyma. Liver part removal reduces segmentation errors only for adjacent right renal parenchyma and segmentation quality for left parenchyma is influenced by spleen tissue that shows similar probability values than renal parenchyma probabilities. Furthermore, we found out that probability map quality produced by our method is superior, particularly, for cortex probability maps (s. Fig. 3). The ref_MLKR are better adapted to the individual parenchymal regions reducing erroneous segmentations into non-parenchymal tissue. Additionally, the variational outer cortex edge alignment force prevents level set evolution into non-parenchymal tissue of adjacent regions (s. Fig. 4). Since related work does not show results for renal parenchyma volumetry in native MRI-data a direct comparison with our method is only possible with the work of [10]. Comparing to the CT data results of [3], who report a mean volume error of 0.048 for right kidney segmentation and the CT data results of [4], who produce a mean volume error of 0.045 (left kidney) and 0.052 (right kidney), our volumetric results are slightly inferior.

6 Conclusion

The proposed methods improve existing segmentation results for fully automatic renal parenchyma volumetry in MR datasets. LDA-based techniques can be used efficiently to generate dimensionality-reduced probability maps considering all available MR weightings. The presented method for MLKR refinement can be applied successfully to calculate segmentation regions that are better adapted to individual

kidney locations of probands. Probability refinement methods improve probability map qualities and provide starting surfaces for final level set segmentations. Particularly, variational techniques offer a great potential to derive forces that can improve level set segmentation results.

Stopping forces (as presented in [10]) can be incorporated as factorial extensions into the level set equation, however, the forces have to be weighted individually to control their combined effects for final level set segmentation results. Instead of combining and coordinating individual alignment forces, variational techniques offer the possibility to derive a single alignment force in an optimization framework. A novel variationally derived outer cortex edge alignment force is presented here, which improves the alignment between the zero level set and the outer cortex edges for renal parenchyma segmentation and produces better volumetric results for epidemiological studies than existing approaches in MR datasets. Since similar tissue properties of adjacent abdominal organs produce similar MR intensities, prior organ shape segmentation models can be stuck in local minima. The presented outer organ edge alignment force reduces the vulnerability of prior organ shape segmentations to produce local minima as suboptimal organ segmentation results.

The proposed MLKR refinement method is developed especially to improve renal parenchyma volumetry results. However, the presented methods for tissue-based probability map generation and variational organ edge alignment show great potential to be applied for other organ segmentations.

7 Acknowledgement

SHIP is part of the Community Medicine Research net of the University of Greifswald, Germany, which is funded by the Federal Ministry of Education and Research, the Ministry of Cultural Affairs as well as the Social Ministry of the Federal State of Mecklenburg-West Pomerania. This work was supported by the ministry for Education, Science and Culture and the European Social Fund (Grant UG 11 035A).

8 Literature

1. Pizer, S., Fletcher P.T, et al.: Deformable m-reps for 3D medical image segmentation. *International Journal of Computer Vision*, 55(2-3), 85-106 (2003)
2. Tsagaan, B., Shimizu, A., Kobatake, H., Miyakawa, K., Hanzawa, Y.: Segmentation of kidney by using a deformable model, *Intern. Conf. on Image Processing 2001*, Thessaloniki (Greece), 1059-1062 , (2001)
3. Kohlberger, T., Uzubas, M.G., Alvino, C., Kadir, T., Slosman, D., Funka-Lea, G.: Organ segmentation with level sets using local shape and appearance priors, *MICCAI 2009*, pp. 34-42, Springer (Heidelberg) 2009
4. Linguraru, M.G., Pura, J.A., Chowdhury, A., Summers, R.M.: Multi-organ segmentation from multi-phase abdominal CT via 4D graphs using enhancement, shape and location optimization. *MICCAI 2010*, pp. 89-96, Springer, Heidelberg (2010)

5. Boykov Y.-Y., Interactive graph cuts for optimal boundary and region segmentation of objects in N-D images, Intern. Conf. on Comp. Vision, pp. 105-112, (2001)
6. Ali, A.M., Farag, A.A., El-Baz, A.S.: Graph cuts framework for kidney segmentation with prior shape constraints, MICCAI 2007, pp. 384-392, Springer, Heidelberg (2007)
7. Sun, Y., Moura, J.M., Yang, D., Ye, Q., Ho, C.: Subpixel registration in renal perfusion MR image sequences. IEEE ISBI 2004, pp. 700-703, (2004)
8. Song, T., Lee, V.S, Rusinek, H., Wong, S., Laine, A.F.: Integrated four dimensional registration and segmentation of dynamic renal MR images. MICCAI 2006, pp. 758-765, Springer, Heidelberg (2006)
9. Yuksel, S.E., El-Baz, A., Farag, A.A., El-Ghar, M., Eldiasty, T., Ghoneim, M.A.: A kidney segmentation framework for dynamic contrast enhanced magnetic resonance imaging, Journal of Vibration and Control, 13(9-10), pp. 1505-1516, 2007.
10. Gloger, O., Tönnies, K., Liebscher, V., Kugelmann, B., Laqua, R., Völzke, H.: Prior Shape Level Set Segmentation on Multi-Step Generated Probability Maps of MR Datasets for Fully Automatic Kidney Parenchyma Volumetry, IEEE Transactions On Medical Imaging, Vol. 31 (2), pp. 312-325, 2012.
11. Hussain, H.K., et al. Hepatic fat fraction: MR imaging for quantitative measurement and display early experience. Radiology (237), pp. 1048-1055 (2005)
12. Cremers, D., Osher, S.J., Soatto, S.: Kernel density estimation and intrinsic alignment for shape priors in level set segmentation. International Journal of Computer Vision, 69(3), pp.335-351, (2006)
13. Fisher, R.: The statistical utilization of multiple measurements, Ann. Eugenics 8, pp. 376-386, (1938)
14. Chan, T., Vese, L.: Active contours without edges. IEEE Transactions on Image Processing, 10(2), pp. 266-277 (2001).